Desalination and Water Treatment
www.deswater.com

doi: 10.5004/dwt.2018.22813

129 (2018) 244–254
October

Two-dimensional zeolitic imidazolate framework-8 for efficient removal of phosphate from water, process modeling, optimization, kinetic, and isotherm studies

Ali Akbar Mohammadi[a], Ahmad Zarei[b], Hossein Alidadi[c,d], Mojtaba Afsharnia[b], Mahmoud Shams[c,d,*]

[a]*Department of Environmental Health Engineering, Neyshabur University of Medical Sciences, Neyshabur, Iran, email: mohammadi.eng73@gmail.com (A.A. Mohammadi)*
[b]*Environmental Health Engineering, School of Health, Gonabad University of Medical Sciences, Gonabad, Iran, emails: a.zarei.tums@gmail.com (A. Zarei), mafsharnia2000@yahoo.com (M. Afsharnia)*
[c]*Social Determinants of Health research center, Mashhad University of Medical Sciences, Mashhad, Iran, emails: shamsmh@mums.ac.ir (M. Shams), alidadih@mums.ac.ir (H. Alidadi)*
[d]*Department of Environmental Health Engineering, School of Health, Mashhad University of Medical Sciences, Mashhad, Iran*

Received 16 January 2018; Accepted 17 July 2018

ABSTRACT

Having unique properties, metal–organic frameworks are recognized as interesting materials for many applications. Leaf-shaped zeolitic imidazolate framework-8 (L-ZIF-8) with a 16.66 m^2/g Brunauer-Emmett-Teller (BET) surface area and total pore volume of 0.0572 cm^3/g was synthesized in aqueous medium and room temperature. L-ZIF-8 then used for P removal from aqueous solutions and a polynomial prediction model for phosphate (P) removal was developed by designing the experiments using central composite design. The model terms showed an increase in P removal with adsorbent dosage and contact time and also by decreasing pH. The highest P removal after model optimization determined to be at pH 4, L-ZIF-8 dosage 0.6 g/L, and 84 min contact time. The isotherm models indicated a monolayer adsorption of P onto L-ZIF-8 with a maximum 51.24 mg P/g of adsorbent. Study of P removal dynamic revealed that the process controlled by chemisorption.

Keywords: Metal organic frameworks; Zeolitic imidazolate framework-8; Adsorption; Phosphorus; Response surface methodology

1. Introduction

Clean water is necessary and vital to life on earth, and recently much attention is concentrated on the supply of clean water for human communities [1–5]. Many industries such as fertilizer, paint and dyes, detergent, corrosion inhibitor, pharmaceutical, and beverage production discharge phosphorous containing effluents in wide range of concentrations [6,7]. Among the industries, fertilizers are the most common which release large quantities of phosphorous [8,9]. Phosphorus is a critical nutrient causing eutrophication of the receiving water, which increases the growth of aquatic plants and algae, with some types of them being potentially toxic [10]. Furthermore, it depletes levels of dissolved oxygen in water and consequently exacerbates water quality. The conventional physical, chemical, and biological methods for phosphorous uptake have some inherent disadvantages, including high costs, post pollution, large quantity of sludge generation, large consumption of chemicals, and low flexibility to wide range of concentrations [11,12]. Therefore, the high levels of phosphorous in effluents should be properly removed before being discharged into the environment, especially water bodies. Among many techniques,

* Corresponding author.

the adsorption process is the most extensively employed method for removal of contaminants due to its environmentally safe process, simple and fast operation, and low cost [13–19]. Exploring new adsorbents with high adsorption capacities is of great importance for the effective adsorption and removal of P from the aquatic environment.

Zeolitic imidazolate frameworks (ZIFs) are a relatively novel subcategory of porous hybrid metal–organic framework (MOF) solids fabricated by the bridging divalent metal cations such as Zn^{+2} and Co^{+2} by imidazolate anions into tetrahedral frameworks [20–23]. MOFs feature exceptional properties such as relatively large surface areas, a wide range of pore sizes, pore configurations, and chemical stability which have received a great attention by researchers in recent years [24,25]. The pore size of ZIFs is in range of nano [24,26,27]. Hence, ZIFs have recently received considerable attention for a variety of application in many fields, such as catalysis, gas adsorption, separation, clean energy, pharmacology, and chemical sensors due facile preparation and excellent thermal and chemical stability in comparison with other classes of MOFs [25,28,29]. One of the most common and extensively focused MOFs is ZIF-8 [30]. Herein, we synthesize a new two-dimensional ZIF with a leaf-shaped morphology named as L-ZIF ($C_{10}H_{16}N_5O_{3/2}$ Zn). L-ZIF is a type of ZIF-8 having same identical building blocks but comprises a unique topology [31,32].

In literature, ZIF-8 has been successfully applied as adsorbent in the uptake of various pollutants such as phthalic acid (H2-PA) and diethyl phthalate [33], *p*-arsanilic acid [34], dye acid blue 40 and methylene blue [35], congo red [36], As(III) and As(V) [37], triiodide anion and rhodamine B molecule [25], and humid acid [38] from aqueous systems.

In this study, it is assumed that L-ZIF-8 can act as a useful adsorbent for separation applications. Therefore, the adsorption feasibility of P from aquatic solution was studied for the first time by conducting batch experiments. Kinetics and isotherm studies of P adsorption onto prepared L-ZIF-8 were thus investigated. Furthermore, the effects of key operational parameters of pH, adsorbent dosage, contact time, and competition anions were examined. Optimization of experimental designs by the traditional procedure of one factor is time consuming, wasting energy and money, and also cannot properly determine the interaction effects between the applied variables [39]. Recently, a growing attention has been focused on response surface methodology (RSM) as an effective approach for optimization of experiments [40]. Thus, in this research, we used RSM based on central composite design (CCD) in "Design-Expert version 7.0.0" software for runs design and statistical analysis. X-ray diffraction (XRD) patterns were taken to determine the phase purity of products and crystallinity of the synthesized L-ZIF-8. Furthermore, the surface morphology of the adsorbent was characterized by a scanning electron microscope (SEM) monograph.

2. Materials and methods

All reagents and chemicals in this research were of analytical grade and were utilized without any purification. $Zn(NO_3)_2$ $6H_2O$ and 2-methylimidazole were acquired from Sigma-Aldrich, Iran. Deionized water was used throughout this work. Leaf-shaped zeolitic imidazolate framework (L-ZIF-8) was prepared using $Zn(NO_3)_2$ $6H_2O$ and 2-methylimidazole (Hmim) in distillated water at room temperature in a manner similar to a method previously published [31]. The molar ratio Hmim/Zn ion (e.g., 8) is a critical factor in shaping the crystals into two dimensions. By applying the exact amounts of Zn ions, L-ZIF-8 yielding above 80% was obtained. The composition analysis of L-ZIF-8 was $C_{10}H_{16}N_5O_{3/2}Zn$. The crystals of synthesized L-ZIF-8 illustrated an exceptional leaf-like morphology with an approximate thickness of 150 nm and a size of about 5 × 2 μm.

2.1. Batch adsorption experiments

The levels of pH, L-ZIF-8 dosage, contact time, and other conditions were selected according to findings obtained from preliminary tests and ranges reported in the literature. The pH values of solutions were adjusted by applying 0.1 mol/L of NaOH or HCl.

2.2. Experimental design and data analysis

In this study, the standard RSM [41] based on CCD was used to measure the optimum conditions for the removal of P by L-ZIF-8. The input parameters chosen for this research were pH (A), adsorbent dosage (B), and time (C) in the ranges of 4–12, 100–1,000 mg/L, and 10–100 min, respectively. For all the runs, the amounts of P concentration (15 mg/L) and agitation speed (250 rpm) were held constant. All the experiments were conducted at 25°C. The removal efficiency of P was considered as the response variable. The designed experiments were evaluated in triplicate with 54 tests in the whole adsorption process. Mathematically, the total number of experiments required for CCD is calculated using the following equation:

$$N = 2^K + 2k + n \tag{1}$$

where N is the total number of experiments, k is the number of variables, and n is repeat of center points [42]. The percentage removal of P by L-ZIF-8 was calculated using the following expression:

$$\text{Removal } \% = \frac{\left(C_{\text{initial}} - C_{\text{final}}\right) \times 100}{C_{\text{initial}}} \tag{2}$$

where C_{initial} is the P concentration before adsorption and C_{final} is the P concentration after adsorption in mg/L. The amount of P adsorbed per gram of L-ZIF-8 at any time t, q_e (mg/g), was evaluated from the following equation:

$$q_e = \frac{\left(C_{\text{initial}} - C_{\text{final}}\right) \times V}{W} \tag{3}$$

where V is the volume of adsorbate in the solution (L), and W is the weight of the used adsorbent (g) [42–44]. The coded values of the input variables were showed as follows:

$$x_i = \frac{X_i - X_0}{\delta_X} \tag{4}$$

where X_i and x_i are the coded and uncoded values of the ith variable, respectively, X_0 stands for the uncoded value of the ith input variable at the center point and δ_X is the value of step change [14,45].

The level and range of coded and uncoded input variables chosen for adsorption study of P are given in Table 1. The modeling and optimization of P removal by L-ZIF-8 was carried out by three chosen input process variables using CCD with 18 designed runs consisting 6 axial points, 8 factorial points, and 4 center points. The obtained data from CCD were evaluated by regression analysis and fitted into the quadratic polynomial model to identify a relationship between the input variables and response:

$$Y = b_0 + \sum_{i=1}^{k} b_i X_i + \sum_{i=1}^{k} b_{ii} X_i^2 + \sum_{i=1}^{k-1} \sum_{i=2}^{k} b_{ij} X_i X_j + \varepsilon \quad (5)$$

In the above equation, Y is the response of the system (P removal), b_0 is a constant value, b_i, b_{ii}, and b_{ij} are the regression coefficients for linear, quadratic, and interactive effects, respectively, Xi and X_j belong to the independent variables, and ε is the random error of the model [46].

Table 1
The level and range of input variables chosen for adsorption study of P from aqueous system using L-ZIF-8

Factor	Code	Variable level				
		–1.525	–1	0	+1	+1.525
pH	A	4	5.4	8	10.6	12
L-ZIF-8 dosage (mg/L)	B	100	254.8	550	845.1	1,000
Contact time (min)	C	10	25.5	55	84.5	100

3. Results and discussion

3.1. Adsorbent characterization

The crystallinity of synthesized L-ZIF-8 was evaluated by the XRD patterns. Fig. 1(a) illustrates the XRD patterns, Fig. 1(b) shows as-synthesized white powder L-ZIF-8, and Fig. 1(c) depicts the SEM image of the L-ZIF-8. The peaks of XRD patterns obtained in this work are similar to those

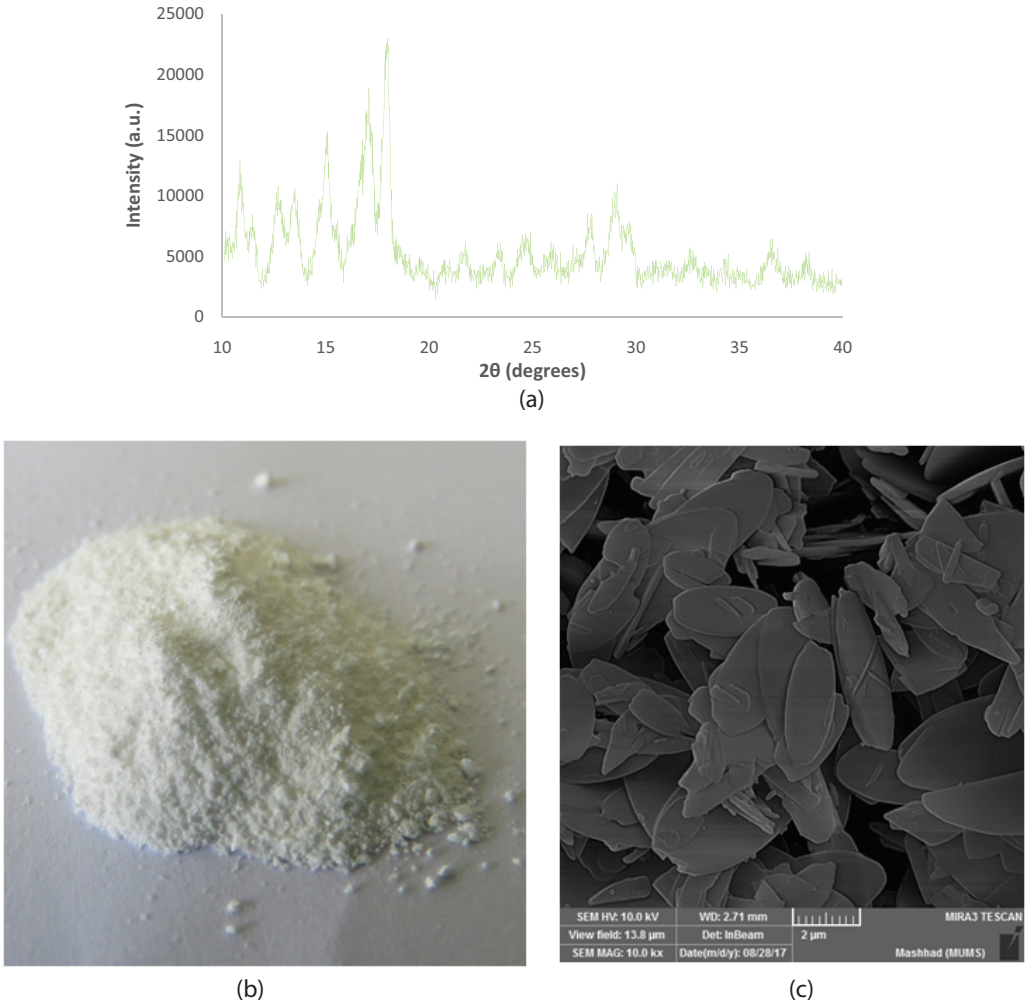

Fig. 1. Characteristics of the as-synthesized L-ZIF-8: (a) XRD pattern, (b) schematic of as-synthesized L-ZIF-8, and (c) SEM micrograph of L-ZIF-8.

reported in literature [31]. The SEM image clearly shows the leaf shape and two-dimensional configuration of the synthesized adsorbent.

BET surface area and total pore volume of the samples were determined from nitrogen adsorption isotherms at 77 K. N_2 adsorption isotherm and pore size distribution of L-ZIF-8 are presented in Table 1 and Fig. 2.

3.2. CCD model for P adsorption

The removal efficiency of P was investigated using an RSM consisted of 18 experimental runs. By performing the experiments according to CCD, the following equation was developed for predicting the P removal by L-ZIF-8:

$$\begin{aligned} \text{P removal}(\%) = {} & 73.82 - 12.53A + 9.67B \\ & + 4.92C - 3.8AB - 1.31AC \\ & + 1.26BC - 1.69A - 1.41B \\ & - 2.81C - 1.96AC - 2.48BC - 3.73BC \end{aligned} \quad (6)$$

where A is the solution pH, B is L-ZIF-8 dosage, and C is the contact time. Positive mark in Eq. (6) represents synergistic influence of the factors, whereas negative mark presents antagonistic effects on P removal. The results of analysis of variance (ANOVA) for the fitted polynomial model are summarized in Table 3. As can be seen in the table, the model terms including A, B, C, AB, AC, BC, A^2, B^2, and C^2 are statistically significant.

The constants of Eq. (6) are obtained from RSM. The accuracy of the suggested model was evaluated by R^2, and its

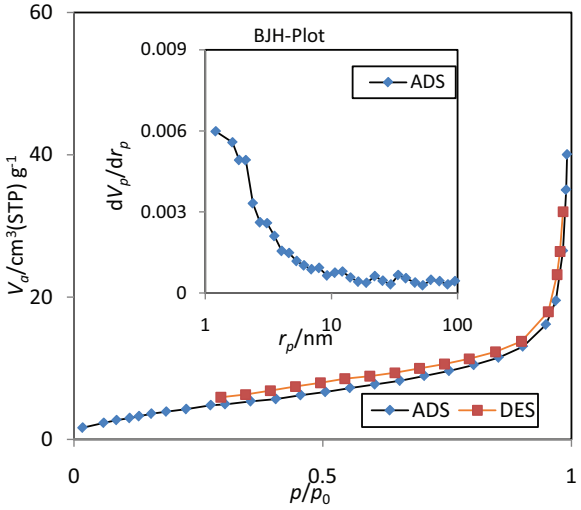

Fig. 2. N_2 adsorption isotherm and pore size distribution of L-ZIF-8.

Table 2
Physical parameters of L-ZIF-8

Parameter	Value
BET surface area (m^2/g)	16.665
Total pore volume (cm^3/g)	0.0572
Mean pore diameter (nm)	13.638

Table 3
Analysis of variance (ANOVA) of the fitted polynomial model for P adsorption by L-ZIF-8

Source	Sum of squares	Df	Mean square	*F*-value	*p*-value	Remarks
Model	3,566.997	12	297.24	131.98	<0.0001	Significant
A-pH	729.62	1	729.62	323.96	<0.0001	Significant
B-dosage	435.12	1	435.12	193.20	<0.0001	Significant
C-time	112.5	1	112.5	49.95	0.0002	Significant
AB	116.28	1	116.28	51.63	0.0002	Significant
AC	13.78	1	13.781	6.12	0.0426	Significant
BC	12.75	1	12.75	5.66	0.0489	Significant
A^2	31.05	1	31.05	13.79	0.0075	Significant
B^2	21.65	1	21.65678	9.61	0.0173	Significant
C^2	85.56	1	85.56	37.99	0.0005	Significant
AC^2	11.29	1	11.29	5.01	0.0601	Not significant
B^2C	18.10	1	18.11	8.04	0.0252	Significant
BC^2	41.05	1	41.05	18.23	0.0037	Significant
Residuals	15.76	7	2.252			
Lack of fit	0.451	2	0.22	0.07	0.9299	Not significant
Pure error	15.31	5	3.06			
Cor total	3,582.76	19				
Standard deviation	1.50		*R*-squared	0.995		
Mean	70.07		Adjusted *R*-squared	0.988		
Coefficient of variation (%)	2.14		Predicted *R*-squared	0.985		
PRESS	51.28		Adequate precision	38.321		

statistical significance was determined by the value of *F* test. The more the amount of R^2, the better is the suggested model. Owning the results of ANOVA in Table 3, it can be stated that the model predictability is at 99% (R^2) confidence interval, implying an excellent fitness of the model in the range of selected variables. This suggested that only 0.01% of all the input variables were not confirmed by this model. Also, the value of adjusted R^2 and predicted R^2 was 0.988 and 0.985, respectively.

P value describes the adequacy of a studied model. Generally, a *p* value lesser than 0.05 represents that the model parameter is significant. The *p* value lesser than 0.0001 in this work indicated that the model terms are statistically significant. Lack of fit value (0.9299) was non-significant illustrating the adequacy of the quadratic model for adsorption of P by L-ZIF-8. *F* and *p* values were applied to describe the importance of the studied parameters in the quadratic model. Furthermore, values of the sum of squares, degrees of freedom, and mean squares were also determined. The amount of *F* value was calculated from dividing mean squares by degrees of freedom; whereas, the mean squares value was derived from dividing sum of squares by degrees of freedom. Adequate precision is the ratio of signal to noise and a ratio greater than 4 is favorable. The value of adequate precision in this study was 38.321, validating the viewpoint mentioned earlier.

The accuracy of the results was evaluated by considering a normal probability plot of the residuals. Generally, the points distributed in the plot should obey a straight line. Fig. 3 shows the experimental vs. predicted, and Fig. 4 shows the normal plot of studentized residuals vs. normal probability for P removal. Experimental vs. predicted adsorption efficiencies for P removal are presented in Table S1.

3.3. Optimization, model validation, and confirmation experiments

In order to maximize the removal percentages of P by L-ZIF-8, optimization analysis was performed. Variable constrains, optimum conditions, and predicted P removal are presented in Table 4. For validation of the optimum predicted levels, some additional experiments were conducted at lab. These experimental results were good agreements with obtained results, representing that the selected quadratic model could predict experimental results properly.

3.4. Determination of isoelectric pH (pHpzc)

Solutions with 0.01 molar NaCl were prepared. Then, the pH value was adjusted in range of 2–12 by adding exact amount of 0.1 N NaOH or 0.1 N HCl. This pH was initial pH (pH_i). A total of 0.2 g of L-ZIF-8 was then added to series of flasks containing 50 mL of NaCl with specified pH, and the suspension was agitated for 48 h. Then, the final pH (pH_f) of supernatant was measured and used to determine the value of pHpzc (Fig. 5). As shown in Fig. 4, the pHpzc of L-ZIF-8 is about 9.3.

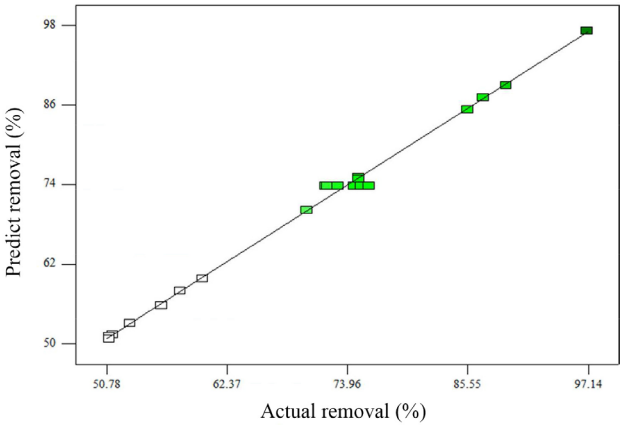

Fig. 3. Experimental vs. predicted adsorption efficiencies for P removal.

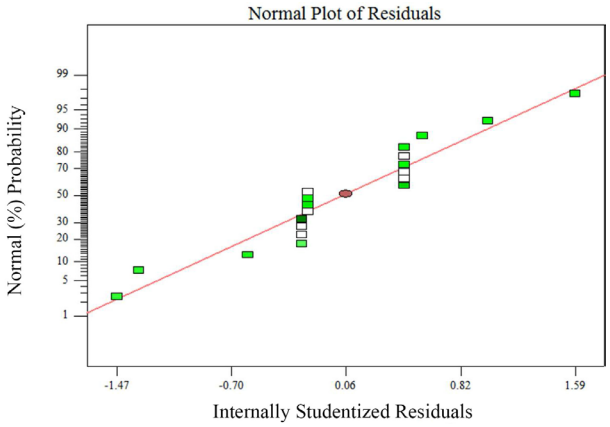

Fig. 4. Normal plot of studentized residuals vs. normal probability for P % removal.

Table 4
Variables constraints and predicted removal optimization of P adsorption by L-ZIF-8 (P: 15 mg/L)

Name	Goal	Constraints			
		Lower limit	Upper limit	Lower weight	Upper weight
pH	Is in range	4	10	1	1
Dosage	Minimize	200	1,000	1	1
Time	Is in range	25.48	84.51	1	1
Removal	Is target = 100	51	100	1	1
Best solution					
pH	Dosage	Time	Removal	Desirability	Experimental removal
4	601.87	84.51	98.24	0.81	96.7 ± 1.9

3.5. Interaction effects of process variables

3.5.1. Effect of pH and adsorbent dosage

The solution pH and applied adsorbent dosage are among the most influential process items for the removal of a contaminant. Adsorption tests were carried out at pH range of 4–12 and adsorbent dosage of 100–1,000 mg/L. The plot of pH vs. adsorbent dosage is presented in Fig. 6. As can be seen in the figure, by increasing the pH value from 4 to 12, the removal efficiency of P decreases which clearly shows the removal of the contaminant is more favorable at lower pHs. ZIF-8 has different functional groups in its structure which induces different charges. Accordingly, at pH < 9.3, ZIF-8 surface was positively charged but at pH > 9.3 its charge changes into negative. This can be the reason for the higher removal efficiency of negative charges of P by positively charged surface of L-ZIF-8 at lower pH. The higher removal efficiency by increasing adsorbent dosage may be due to the availability of more adsorbing binding sites on the adsorbent surface.

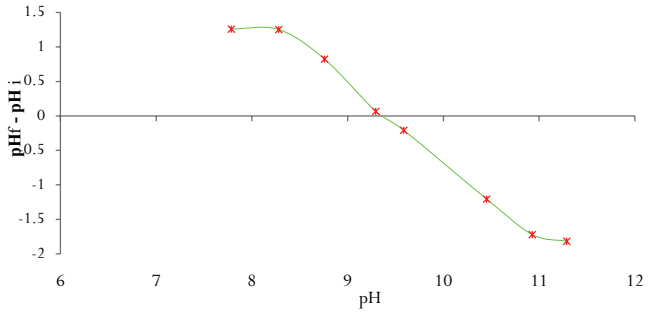

Fig. 5. The pHpzc of L-ZIF-8.

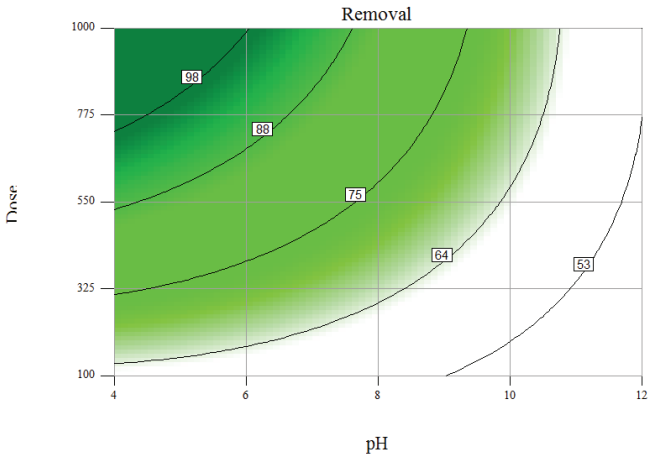

Fig. 6. Combined effect of pH and adsorbent dosage on P adsorption by L-ZIF-8.

3.5.2. Effect of pH and contact time

The contact time to reach a desirable removal has a high influence in the size of the real treating units and thus the economy of sorption system. Combined effect of pH and contact time on adsorption of P by L-ZIF-8 is depicted in Fig. 7. As shown in the figure, the L-ZIF-8 is a very fast adsorbent toward P. The P uptake increased by time, consequently of having more time for P ions to penetrate into L-ZIF-8 pores.

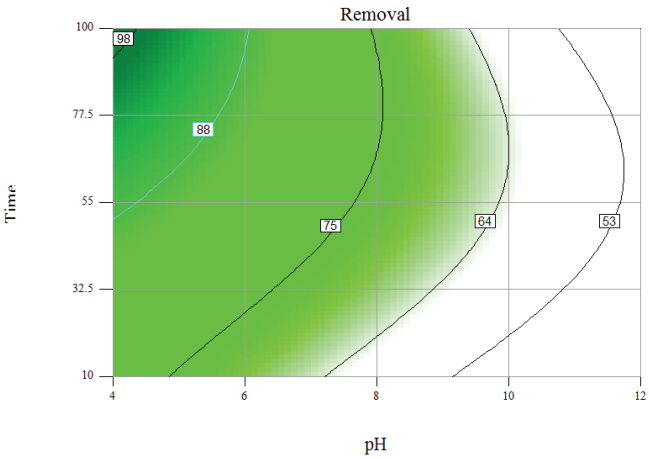

Fig. 7. Combined effect of pH and contact time on P adsorption by L-ZIF-8.

Table 5
The parameters of fitted models for P adsorption equilibrium data

Isotherm	Formula	Linear form	Parameter	Value
Langmuir	$q_e = \frac{q_m b C_e}{1 + bC_e}$	$\frac{C_e}{q_e} = \frac{1}{q_m} C_e + \frac{1}{q_m b}$	q_{max} (mg/g)	51.24
			K_L (L/mg)	1.5
			R^2	0.99
Freundlich	$q_e = K_F C_e^{1/n}$	$\log q_e = \log K_F + \frac{1}{n} \log C_e$	K_F (mg/g(L/mg)$^{1/n}$	3.42
			n	25.9
			R^2	0.98
Temkin	$q_e = \frac{RT}{b} \ln(k_T C_e)$	$q_e = B_1 ln.k_t + B_1 \ln C_e$	k_t (L/mg)	0.51
			B_1	6.41
			R^2	0.90
Dubinin–Radushkevich	$q_e = q_m exp(-\beta\varepsilon^2)$	$\ln q_e = \ln q_m - \beta\epsilon^2$	q_{max} (mg/g)	33.5
			β	1.4
			R^2	0.76

3.6. Sorption isotherm

The Langmuir, Freundlich, Temkin, and Dubinin–Radushkevich isotherms [47–49] were applied to investigate the adsorption behavior of P by L-ZIF-8. The isotherm study was conducted by changing the initial concentration of the contaminant from 5 to 40 mg/L at a constant adsorbent dosage of 0.625 g/L. The parameters and graphical presentation of fitted models are shown in Table 5 and Figs. 8(a)–(d), respectively.

As shown in Table 5, Langmuir model described the equilibrium data well. The Langmuir isotherm is based on two assumptions: First, the adsorbate molecules cover the adsorbent surface as a monolayer form. Secondly, the model considers a homogenously distributed sorption sites on the adsorbent that have same binding energies [50]. A comparison of different adsorbents used for P removal is given in Table 6. As seen, L-ZIF-8 has a higher monolayer adsorbent capacity (q_{max}) comparing many of adsorbents reported in the literature, including our previous work on P adsorption by cubic ZIF-8 [20].

From the Langmuir isotherm, a dimensionless parameter has been developed that exhibits the essential features of the sorption process. Separation factor (K_R) can be obtained from Eq. (7) and reveals the sorption process to be unfavorable ($K_R > 1$), linear ($K_R = 1$), favorable ($0 < K_R < 1$), or irreversible ($K_R = 0$).

$$K_R = \frac{1}{1 + K_L C_0} \tag{7}$$

where K_L is the Langmuir constant and C_0 is the initial P concentration. Table 7 shows a K_R range between 0.1 and 0.01 for P removal by L-ZIF-8. These values for K_R indicate the favorability of P sorption by L-ZIF-8.

Table 6
A comparison between various adsorbents used for P removal

Adsorbent	Q_0 (mg/g)	Reference
Humic acid-coated magnetite nanoparticles	28.9	[51]
Magnetic iron oxide nanoparticles	5.03	[52]
Poly(vinyl alcohol) (PVA) hydrogel beads	11.5	[53]
Hydrous zirconium oxide (HZO) embedded in quaternary-ammonium Chinese reed	59.2	[54]
Lanthanum-incorporated porous zeolite	17.2	[55]
Fe–Mn oxide adsorbent	18.4	[56]
Zirconium-modified activated carbon nanofiber	26.3	[57]
Zero valent iron (ZVI)	35	[58]
Cross-linked chitosan bead	52.1	[59]
Nanostructured iron(III)–copper(II) binary oxides	35.2	[60]
Cubic zeolitic imidazolate framework-8	38.22	[20]
L-ZIF-8	51.24	Present work

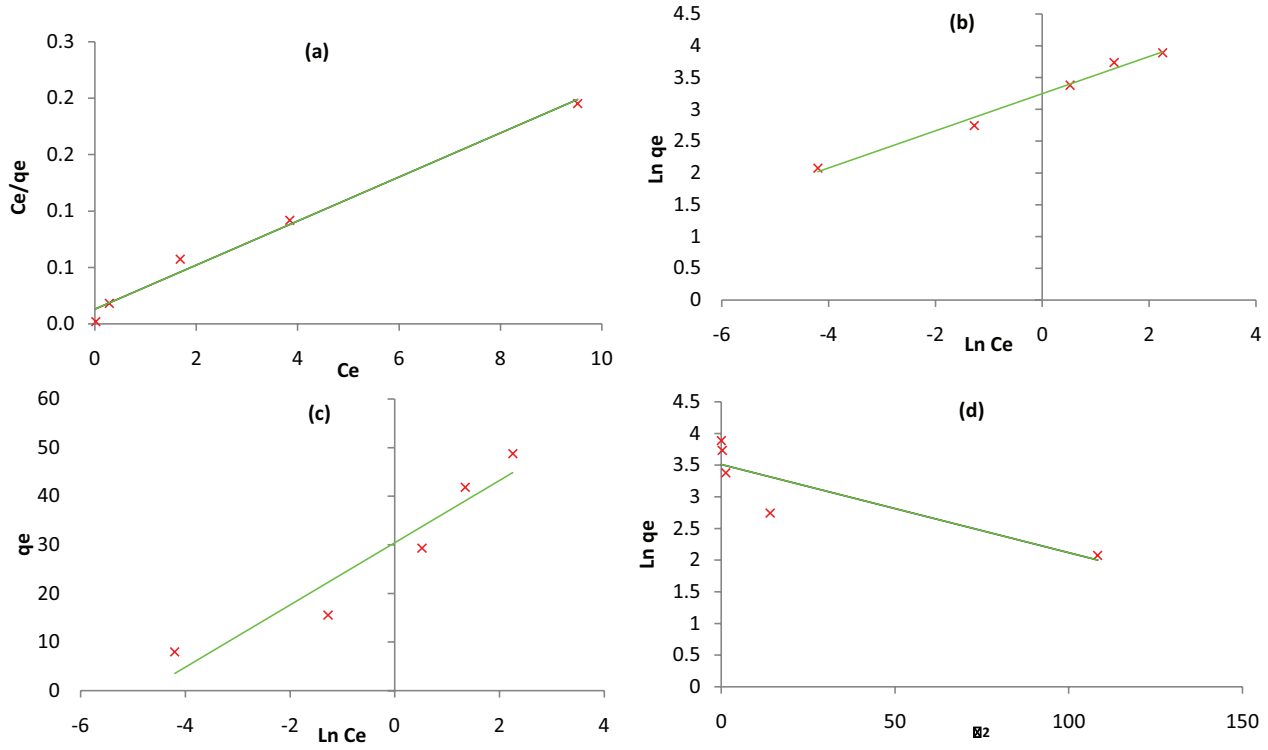

Fig. 8. Fitting the experimental data with (a) Langmuir, (b) Freundlich, (c) Temkin, and (d) Dubinin–Radushkevich models.

3.7. Sorption kinetics

The kinetic study of the adsorption of P by L-ZIF-8 was carried out, and results were analyzed with kinetic models. Equations of pseudo-first-order kinetic model, pseudo-second-order kinetic model, and intra-particle diffusion kinetic [61] are given in Table 8. The table shows the coefficients for the kinetic models. The kinetic graphs are also illustrated in Fig. 9. Pseudo-second-order kinetic model with higher R^2 values in most cases was the most appropriate among the studied models, an indication of chemisorption as a rate limiting step in sorption process.

Table 7
Separation factor (K_R) for different initial P concentrations

Initial P concentration (mg/L)	K_R
5	0.117
10	0.062
20	0.032
30	0.0217
40	0.016

4. Conclusions

In this study, we have prepared a leaf-shaped ZIF-8 in a simple and green synthesis method in aqueous media at room temperature. The results of this study suggested that P removal by L-ZIF-8 is strongly affected by parameters such as pH, adsorbent dosage, and contact time. Among the various models examined, Langmuir isotherm model was found to give the best fit to the experimental data, demonstrating a monolayer adsorption with a maximum adsorption capacity of 51.24 mg P/g of adsorbent. The study of adsorption kinetics also indicated that the process was in good agreement with the second-order kinetic model. Use of green approach in the synthesis of L-ZIF-8, high yield of L-ZIF-8 synthesis, rapid adsorption, and high capacity of L-ZIF-8 for P, all makes L-ZIF-8 an exceptional candidate for use as adsorbent for P removal.

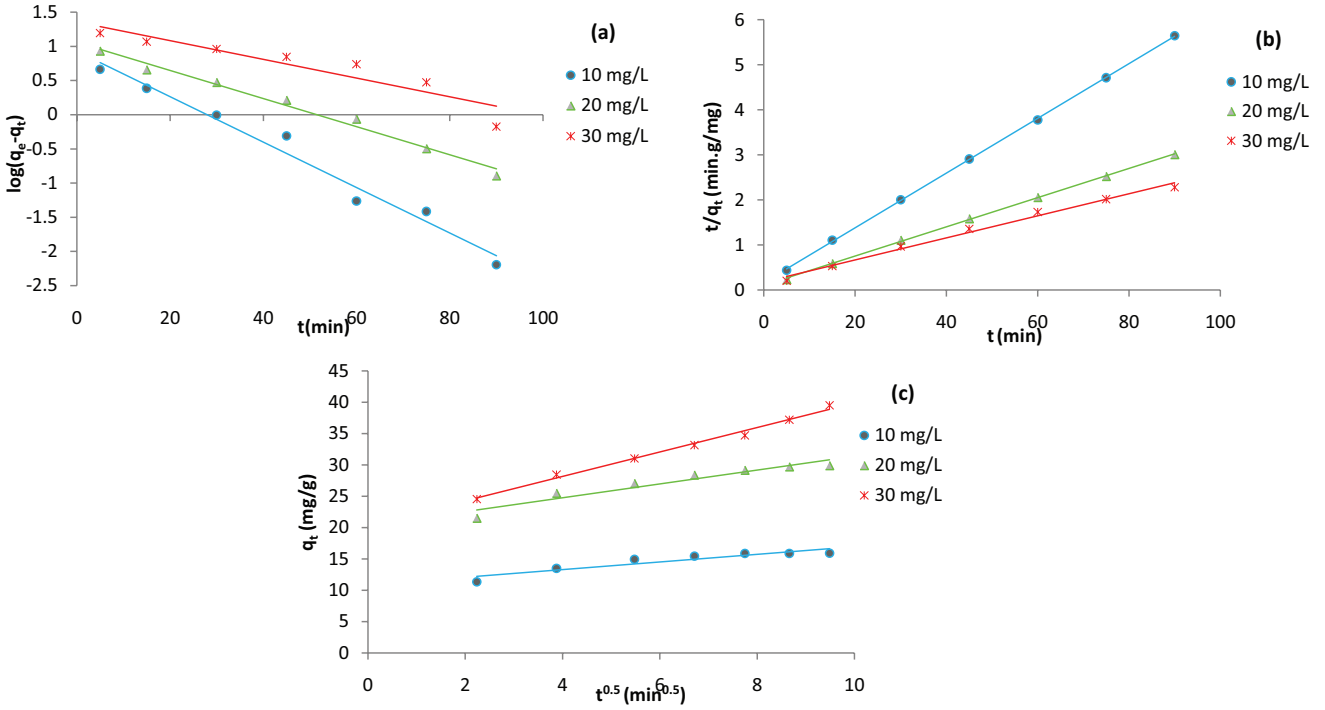

Fig. 9. Kinetic models studied for P removal by L-ZIF-8: (a) pseudo-first-order, (b) pseudo-second-order, and (c) intra-particle diffusion kinetic models.

Table 8
Parameters of kinetic models fitted to P adsorption experiments

C_0 (mg/L)	$q_{e,exp}$ (mg/g)	Pseudo first order $\log(q_e - q_t) = \log q_e - \frac{k_1}{2.303}.t$			Pseudo second order $\frac{t}{q_t} = \frac{1}{k_2 qe^2} + \frac{1}{q_e}.t$			Intra-particle diffusion $q_t = k_p.t^{0.5} + c$	
		$q_{e,cal}$ (mg/g)	K_1 (min^{-1})	R^2	$q_{e,cal}$ (mg/g)	K_2 (min^{-1})	R^2	K_p (mg/g. min$^{-0.5}$)	R^2
10	15.94	8.43	0.08	0.98	16.47	0.02	0.99	0.6	0.92
20	30.04	10.4	0.04	0.87	30.65	0.01	0.99	1.1	0.99
30	40.17	17.4	0.07	0.98	38.4	0.005	0.99	1.94	0.92

Acknowledgment

This work is funded by the Neyshabur University of Medical Science, Iran.

References

[1] M. Ghaderpoori, M. Paydar, A. Zarei, H. Alidadi, A.A. Najafpoor, A.H. Gohary, M. Shams, Health risk assessment of fluoride in water distribution network of Mashhad, Iran, Hum. Ecol. Risk Assess., 24 (2018) 1–12.
[2] R. Khosravi, A. Zarei, M. Heidari, A. Ahmadfazeli, M. Vosughi, M. Fazlzadeh, Application of ZnO and TiO_2 nanoparticles coated onto montmorillonite in the presence of H_2O_2 for efficient removal of cephalexin from aqueous solutions, Korean J. Chem. Eng., 35 (2018) 1–9.
[3] M.H. Dehghani, M. Farhang, M. Alimohammadi, M. Afsharnia, G. Mckay, Adsorptive removal of fluoride from water by activated carbon derived from $CaCl_2$-modified *Crocus sativus* leaves: equilibrium adsorption isotherms, optimization, and influence of anions, Chem. Eng. Commun., 205 (2018) 1–11.
[4] M. Shams, R.N. Nodehi, M. Alimohammadi, A. Mahvi, A survey of nitrate and fluoride in water distribution networks of Tabas, Iran, World Appl. Sci. J., 7 (2009) 1516–1520.
[5] M. Dehghani, M. Farhang, A. Zarei, Investigation of carbonyl compounds (acetaldehyde and formaldehyde) in bottled waters in Iranian markets, Int. Food Res. J., 25 (2018) 876–879.
[6] K. Karageorgiou, M. Paschalis, G.N. Anastassakis, Removal of phosphate species from solution by adsorption onto calcite used as natural adsorbent, J. Hazard. Mater., 139 (2007) 447–452.
[7] M. Fahiminia, A. Paksa, A. Zarei, M. Shams, H. Bakhtiari, M. Norouzi, Survey of optimal methods for the control of cockroaches in sewers of Qom City, Iran. J. Health Environ., 3 (2010) 19–26.
[8] Q. Xie, Y. Li, Z. Lv, H. Zhou, X. Yang, J. Chen, H. Guo, Effective adsorption and removal of phosphate from aqueous solutions and eutrophic water by Fe-based MOFs of MIL-101, Sci. Rep., 7 (2017) 3316.
[9] M.H. Dehghani, G.-R. Jahed, A. Zarei, Investigation of low-pressure ultraviolet radiation on inactivation of *Rhabitidae nematode* from water, Iran. J. Public Health, 42 (2013) 314.
[10] K.A. Krishnan, A. Haridas, Removal of phosphate from aqueous solutions and sewage using natural and surface modified coir pith, J. Hazard. Mater., 152 (2008) 527–535.
[11] Z. Wen, Y. Zhang, C. Dai, Removal of phosphate from aqueous solution using nanoscale zerovalent iron (nZVI), Colloids Surf., A, 457 (2014) 433–440.
[12] M. Shams, I. Nabipour, S. Dobaradaran, B. Ramavandi, M. Qasemi, M. Afsharnia, An environmental friendly and cheap adsorbent (municipal solid waste compost ash) with high efficiency in removal of phosphorus from aqueous solution, Fresenius Environ. Bull., 22 (2013) 723–727.
[13] M. Fazlzadeh, K. Rahmani, A. Zarei, H. Abdoallahzadeh, F. Nasiri, R. Khosravi, A novel green synthesis of zero valent iron nanoparticles (NZVI) using three plant extracts and their efficient application for removal of Cr (VI) from aqueous solutions, Adv. Powder Technol., 28 (2017) 122–130.
[14] M. Shams, M. Qasemi, M. Afsharnia, A. Hossein Mahvi, Sulphate removal from aqueous solutions by granular ferric hydroxide, Desal. Wat. Treat., 57 (2016) 23800–23807.
[15] M. Shams, M. Qasemi, A. Mahvi, S. Dobaradaran, Defluoridation of aqueous solutions with waste aluminum filings, Fluoride, 45 (2012) 197.
[16] A. Naghizadeh, H. Shahabi, F. Ghasemi, A. Zarei, Synthesis of walnut shell modified with titanium dioxide and zinc oxide nanoparticles for efficient removal of humic acid from aqueous solutions, J. Water Health, 14 (2016) 989–997.
[17] Z. Yang, W. Liu, H. Zhang, X. Jiang, F. Min, DFT study of the adsorption of 3-chloro-2-hydroxypropyl trimethylammonium chloride on montmorillonite surfaces in solution, Appl. Surf. Sci., 436 (2018) 58–65.
[18] I.-H. Liao, J.-H. Huang, S.-L. Wang, M.-P. Cheng, J.-C. Liu, Adsorptions of Cd(II) and Pb(II) in aqueous solution by rice-straw char, Desal. Wat. Treat., 57 (2016) 21619–21626.
[19] J. Hizal, P. Demirçivi, Ş. Karadirek, R. Apak, Investigation of individual and competitive adsorption of Cu (II), Cd (II), and Pb (II) on montmorillonite in terms of surface complexation and kinetic properties of Cu(II) adsorption, Desal. Wat. Treat., 57 (2016) 22441–22453.
[20] M. Shams, M.H. Dehghani, R. Nabizadeh, A. Mesdaghinia, M. Alimohammadi, A.A. Najafpoor, Adsorption of phosphorus from aqueous solution by cubic zeolitic imidazolate framework-8: modeling, mechanical agitation vs. sonication, J. Mol. Liq., 224 (2016) 151–157.
[21] N.L. Torad, Y. Li, S. Ishihara, K. Ariga, Y. Kamachi, H.-Y. Lian, H. Hamoudi, Y. Sakka, W. Chaikittisilp, K.C.-W. Wu, MOF-derived nanoporous carbon as intracellular drug delivery carriers, Chem. Lett., 43 (2014) 717–719.
[22] E. Haque, J.W. Jun, S.H. Jhung, Adsorptive removal of methyl orange and methylene blue from aqueous solution with a metal-organic framework material, iron terephthalate (MOF-235), J. Hazard. Mater., 185 (2011) 507–511.
[23] S.-H. Huo, X.-P. Yan, Metal–organic framework MIL-100 (Fe) for the adsorption of malachite green from aqueous solution, J. Mater. Chem., 22 (2012) 7449–7455.
[24] X. Fan, L. Yu, L. Li, C. Yang, J. Wen, X. Ye, J. Cheng, Y. Hu, Characterization and application of zeolitic imidazolate framework-8@ polyvinyl alcohol nanofibers mats prepared by electrospinning, Mater. Res. Express, 4 (2017) 026404.
[25] X. Fan, W. Wang, W. Li, J. Zhou, B. Wang, J. Zheng, X. Li, Highly porous ZIF-8 nanocrystals prepared by a surfactant mediated method in aqueous solution with enhanced adsorption kinetics, ACS Appl. Mater. Interfaces, 6 (2014) 14994–14999.
[26] J.A. Thompson, K.W. Chapman, W.J. Koros, C.W. Jones, S. Nair, Sonication-induced Ostwald ripening of ZIF-8 nanoparticles and formation of ZIF-8/polymer composite membranes, Microporous Mesoporous Mater., 158 (2012) 292–299.
[27] N. Bakhtiari, S. Azizian, Adsorption of copper ion from aqueous solution by nanoporous MOF-5: a kinetic and equilibrium study, J. Mol. Liq., 206 (2015) 114–118.
[28] J. Kim, B. Chen, T.M. Reineke, H. Li, M. Eddaoudi, D.B. Moler, M. O'Keeffe, O.M. Yaghi, Assembly of metal–organic frameworks from large organic and inorganic secondary building units: new examples and simplifying principles for complex structures, J. Am. Chem. Soc., 123 (2001) 8239–8247.
[29] M. Massoudinejad, M. Ghaderpoori, A. Shahsavani, M.M. Amini, Adsorption of fluoride over a metal organic framework Uio-66 functionalized with amine groups and optimization with response surface methodology, J. Mol. Liq., 221 (2016) 279–286.
[30] J. Cravillon, S. Münzer, S.-J. Lohmeier, A. Feldhoff, K. Huber, M. Wiebcke, Rapid room-temperature synthesis and characterization of nanocrystals of a prototypical zeolitic imidazolate framework, Chem. Mater., 21 (2009) 1410–1412.
[31] R. Chen, J. Yao, Q. Gu, S. Smeets, C. Baerlocher, H. Gu, D. Zhu, W. Morris, O.M. Yaghi, H. Wang, A two-dimensional zeolitic imidazolate framework with a cushion-shaped cavity for CO_2 adsorption, Chem. Commun., 49 (2013) 9500–9502.
[32] M.J. Chen, A.C. Yang, N.H. Wang, H.C. Chiu, Y.L. Li, D.Y. Kang, S.L. Lo, Influence of crystal topology and interior surface functionality of metal-organic frameworks on PFOA sorption performance, Microporous Mesoporous Mater., 236 (2016) 202–210.
[33] N.A. Khan, B.K. Jung, Z. Hasan, S.H. Jhung, Adsorption and removal of phthalic acid and diethyl phthalate from water with zeolitic imidazolate and metal–organic frameworks, J. Hazard. Mater., 282 (2015) 194–200.
[34] B.K. Jung, J.W. Jun, Z. Hasan, S.H. Jhung, Adsorptive removal of p-arsanilic acid from water using mesoporous zeolitic imidazolate framework-8, Chem. Eng. J., 267 (2015) 9–15.
[35] X.Z. Kang, Z.W. Song, Q. Shi, J.X. Dong, Utilization of zeolite imidazolate framework as an adsorbent for the removal of dye from aqueous solution, Asian J. Chem., 25 (2013) 8324.
[36] C. Jiang, B. Fu, H. Cai, T. Cai, Efficient adsorptive removal of Congo red from aqueous solution by synthesized zeolitic

imidazolate framework-8, Chem. Speciation Bioavailability, 28 (2016) 199–208.
[37] M. Jian, B. Liu, G. Zhang, R. Liu, X. Zhang, Adsorptive removal of arsenic from aqueous solution by zeolitic imidazolate framework-8 (ZIF-8) nanoparticles, Colloids Surf., A, 465 (2015) 67–76.
[38] H. Guo, F. Lin, J. Chen, F. Li, W. Weng, Metal–organic framework MIL-125 (Ti) for efficient adsorptive removal of Rhodamine B from aqueous solution, Appl. Organomet. Chem., 29 (2015) 12–19.
[39] R.H. Myers, D.C. Montgomery, G.G. Vining, C.M. Borror, S.M. Kowalski, Response surface methodology: a retrospective and literature survey, J. Qual. Technol., 36 (2004) 53.
[40] J. Marrugo-Negrete, J. Pinedo-Hernández, J. Baeza-Reyes, Optimization of the electrodeposition conditions for mercury removal from vegetal biomass with response surface methodology, Portugaliae Electrochim. Acta, 31 (2013) 107–117.
[41] M.H. Dehghani, A. Zarei, A. Mesdaghinia, R. Nabizadeh, M. Alimohammadi, M. Afsharnia, Response surface modeling, isotherm, thermodynamic and optimization study of arsenic (V) removal from aqueous solutions using modified bentonite-chitosan (MBC), Korean J. Chem. Eng., 34 (2017) 757–767.
[42] Y. Yasin, M. Mohamad, F.B. Ahmad, The application of response surface methodology for lead ion removal from aqueous solution using intercalated tartrate-Mg-Al layered double hydroxides, Int. J. Chem. Eng., 2013 (2013) 1–7.
[43] M. Shams, R.N. Nodehi, M. Dehghani, M. Younesian, A. Mahvi, Efficiency of granular ferric hydroxide (GFH) in fluoride removal from water, Fluoride, 43 (2009) 35–40.
[44] M.H. Dehghani, A. Zarei, A. Mesdaghinia, R. Nabizadeh, M. Alimohammadi, M. Afsharnia, Adsorption of Cr (VI) ions from aqueous systems using thermally sodium organo-bentonite biopolymer composite (TSOBC): response surface methodology, isotherm, kinetic and thermodynamic studies, Desalin. Water Treat., 85 (2017) 298–312.
[45] M. Fazlzadeh, R. Khosravi, A. Zarei, Green synthesis of zinc oxide nanoparticles using *Peganum harmala* seed extract, and loaded on *Peganum harmala* seed powdered activated carbon as new adsorbent for removal of Cr (VI) from aqueous solution, Ecol. Eng., 103 (2017) 180–190.
[46] R. Wiens, M. Rak, J. Sedlmair, C. Hirschmugl, J. Morrison, C. Mundy, M. Kansiz, K. Gough, Rapid biodiagnostic ex vivo imaging at 1 μm pixel resolution with thermal source FTIR FPA, Analyst, 140 (2015) 2493–2503.
[47] O. Rahmanian, M. Dinari, M.K. Abdolmaleki, Carbon quantum dots/layered double hydroxide hybrid for fast and efficient decontamination of Cd (II): the adsorption kinetics and isotherms, Appl. Surf. Sci., 428 (2018) 272–279.
[48] M.H. Dehghani, E. Nikfar, A. Zarei, N.M. Esfahani, The effects of US/H2O2 processes on bisphenol-A toxicity in aqueous solutions using *Daphnia magna*, Desalin. Water Treat., 68 (2017) 183–189
[49] M. Qasemi, M. Afsharnia, A. Zarei, A.A. Najafpoor, S. Salari, M. Shams, Phenol removal from aqueous solution using *Citrullus colocynthis* waste ash, Data Brief, 18 (2018) 620–628.
[50] N. Mirzaei, H.R. Ghaffari, K. Sharafi, A. Velayati, G. Hoseindoost, S. Rezaei, A.H. Mahvi, A. Azari, K. Dindarloo, Modified natural zeolite using ammonium quaternary based material for Acid red 18 removal from aqueous solution, J. Environ. Chem. Eng., 5 (2017) 3151–3160.
[51] M. Rashid, N.T. Price, M.Á.G. Pinilla, K.E. O'Shea, Effective removal of phosphate from aqueous solution using humic acid coated magnetite nanoparticles, Water Res., 123 (2017) 353–360.
[52] S.Y. Yoon, C.G. Lee, J.A. Park, J.H. Kim, S.B. Kim, S.H. Lee, J.W. Choi, Kinetic, equilibrium and thermodynamic studies for phosphate adsorption to magnetic iron oxide nanoparticles, Chem. Eng. J., 236 (2014) 341–347.
[53] B. Hui, Y. Zhang, L. Ye, Preparation of PVA hydrogel beads and adsorption mechanism for advanced phosphate removal, Chem. Eng. J., 235 (2014) 207–214.
[54] Y. Shang, X. Xu, S. Qi, Y. Zhao, Z. Ren, B. Gao, Preferable uptake of phosphate by hydrous zirconium oxide nanoparticles embedded in quaternary-ammonium Chinese reed, J. Colloid Interface Sci., 496 (2017) 118–129.
[55] Y. He, H. Lin, Y. Dong, L. Wang, Preferable adsorption of phosphate using lanthanum-incorporated porous zeolite: characteristics and mechanism, Appl. Surf. Sci., 426 (2017) 995–1004.
[56] X. Du, Q. Han, J. Li, H. Li, The behavior of phosphate adsorption and its reactions on the surfaces of Fe–Mn oxide adsorbent, J. Taiwan Inst. Chem. Eng., 76 (2017) 167–175.
[57] W. Xiong, J. Tong, Z. Yang, G. Zeng, Y. Zhou, D. Wang, P. Song, R. Xu, C. Zhang, M. Cheng, Adsorption of phosphate from aqueous solution using iron-zirconium modified activated carbon nanofiber: performance and mechanism, J. Colloid Interface Sci., 493 (2017) 17–23.
[58] N. Sleiman, V. Deluchat, M. Wazne, M. Mallet, A. Courtin-Nomade, V. Kazpard, M. Baudu, Phosphate removal from aqueous solutions using zero valent iron (ZVI): Influence of solution composition and ZVI aging, Colloids Surf., A, 514 (2017) 1–10.
[59] M.H. Mahaninia, L.D. Wilson, Phosphate uptake studies of cross-linked chitosan bead materials, J. Colloid Interface Sci., 485 (2017) 201–212.
[60] G. Zhang, Z. Ren, X. Zhang, J. Chen, Nanostructured iron (III)-copper (II) binary oxide: a novel adsorbent for enhanced arsenic removal from aqueous solutions, Water Res., 47 (2013) 4022–4031.
[61] F. Raji, M. Pakizeh, Kinetic and thermodynamic studies of Hg (II) adsorption onto MCM-41 modified by ZnCl 2, Appl. Surf. Sci., 301 (2014) 568–575.

Supplementary

Table S1
Experimental design and results for P removal by L-ZIF-8

Run no.	Coded variable			Response (% removal)	
	A	B	C	Observed	Predicted
1	0	0	0	71.8	73.8
2	–1	1	1	97	97.1
3	–1	–1	1	75	75.1
4	–1	1	–1	87	87.1
5	0	–1.5	0	56	55.8
6	1	–1	1	51	51.2
7	0	0	0	76	73.8
8	–1	–1	–1	70	70.2
9	0	1.5	0	85.5	85.3
10	0	0	0	72	73.8
11	0	0	1.5	75	74.8
12	1	1	–1	53	53.2
13	–1.5	0	0	89.2	89
93	0	0	0	74.6	73.8
15	0	0	0	75.2	73.8
16	0	0	–1.5	60	59.8
17	0	0	0	73	73.8
18	1.5	0	0	51	50.8
88.5	1	1	1	57	57.9
73.8	1	–1	–1	51	51.4